THE AMERICAN SOCIETY OF MECHANICAL ENGINEERS
345 E. 47th St., New York, N.Y. 10017

98-GT-71

THE INFLUENCE OF ENDWALL CONTOURING ON THE PERFORMANCE OF A TURBINE NOZZLE GUIDE VANE

Vincenzo Dossena
Dipartimento di Energetica, Politecnico di Milano
Piazza Leonardo da Vinci 32, 20133 Milano, Italy

Antonio Perdichizzi and **Marco Savini**
Facoltà di Ingegneria, Università di Bergamo
Viale G. Marconi 5, 24044 Dalmine (Bg), Italy

ABSTRACT

The paper presents the results of a detailed investigation of the flow field in a gas turbine linear cascade. A comparison between a contoured and a planar configuration of the same cascade has been performed, and differences in the three-dimensional flow field are here analyzed and discussed. The flow evolution downstream of the trailing edge was surveyed by means of probe traversing while a 3-D Navier-Stokes solver was employed to obtain information on flow structures inside the vaned passages. The experimental measurements and the numerical simulation of the three-dimensional flow field has been performed for two cascades; one with planar endwalls, and the other with one planar and one profiled endwall, so as to present a reduction of the nozzle height. The investigation was carried out at an isentropic downstream Mach number of 0.6. Airfoils of both cascades were scaled from the same high pressure gas turbine inlet guide vane. Measurements of the three-dimensional flow field have been performed on five planes downstream of the cascades by means of a miniaturized five-hole pressure probe. The presence of endwall contouring strongly influences the secondary effects; the vortex generation and their development is inhibited by the stronger acceleration taking place throughout the cascade. The results show that the secondary effects on the contoured side of the passage are confined in the endwall region, while on the flat side the secondary vortices display characteristics similar to the ones occurring downstream of the planar cascade. The spanwise outlet angle distribution presents a linear variation for most of the nozzle height, with quite low values approaching the contoured endwall. The analysis of mass averaged losses shows a significant performance improvement in the contoured cascade. This has to be ascribed not only to lower secondary losses but also to a reduction of the profile losses.

NOMENCLATURE

b	= axial chord
c	= chord
Cps	= static pressure coefficient = $(pt_1-p)/(pt_1-p_2)$
Cpt	= total pressure coefficient = $(pt_1-pt)/(pt_1-p_2)$
h	= height
M	= Mach Number
p	= pressure
pt	= total pressure
Re	= Reynolds Number
s	= pitch
x, y, z	= axial, pitchwise and spanwise coordinate
β	= flow angle with respect to tangential direction
ω	= vorticity

Subscripts

1	= inlet
2	= exit
d	= design
ov	= overall
is	= isentropic
s	= streamwise
t	= total

Presented at the International Gas Turbine & Aeroengine Congress & Exhibition
Stockholm, Sweden — June 2–June 5, 1998
This paper has been accepted for publication in the Transactions of the ASME
Discussion of it will be accepted at ASME Headquarters until September 30, 1998

INTRODUCTION

In the development of advanced gas turbines one of the most effective methods to improve the turbine performance is the adoption of fully 3-D design both for stator vanes and rotor blades. Complex geometries, suggested by a better knowledge of the flow field, can often produce a reduction of aerodynamic losses. A very delicate task is the design of high pressure turbine vane; not only because of the well known cooling problems, but also because of the high aerodynamic losses: in fact the first vane is characterized by low aspect ratios and, due to cooling requirements, the pitch-chord ratio is generally high. Both these features act to enhance the secondary flow intensity, so that secondary losses become of the same order of magnitude as the profile losses, or even predominant. A technique to lessen the losses is endwall contouring. In modern gas turbines, the transition between the combustion chamber and the turbine inlet requires a reduction of the flow passage area, and this may be accomplished by profiling the casing in the first vane.

Many authors have shown that endwall contouring is an effective tool to improve the vane efficiency. Dejc et al, (1965) proposed design rules for meridional tip endwall contouring, indicating the optimum contraction ratio for a given aspect ratio, and reported on efficiency increases in rotating rigs. The improvements were related to the major acceleration due to the greater channel convergence, that reduces profile losses and inhibits the secondary flow development. Ewen et al. (1973) investigated the aerodynamic performance of a small axial stage turbine, concluding that the efficiency increase was related mostly to improved rotor inlet conditions and to a higher degree of reaction. Morris and Hoare (1975) performed tests at low velocity on linear cascades with different endwall geometries; the correlation they developed on the basis of the results showed a significant loss reduction, even if its amount was much less than the one predicted by Dejic. Kopper et al. (1981) carried out an investigation on a cascade with one contoured endwall, at an exit Mach number of 0.85. Comparison with the planar endwall configuration surprisingly showed that most of the improvement occurred on the flat half span. Boletis (1985) performed a detailed analysis of the flow field in an annular cascade with meridional tip endwall contouring at low velocity conditions. Besides the expected overall losses decrease, the whole flow field was found to be positively affected by tip contouring. Not only the pitchwise pressure gradient in the front part of the cascade is significantly reduced, thus causing lower secondary losses, but even in the rear part of the profile the endwall curvature is beneficial. In fact it produces a low pressure region at the tip, counteracting the radial pressure gradient imposed by the annular configuration; as a result there is a minor inward migration of low-momentum fluid which causes a contraction of the wake region. These findings were substantially confirmed by the work of Moustapha et al. (1986), where two different endwall shape, with the same height contraction, were investigated. The nozzle characterized by a more rapid contraction and tip back curvature, exhibited a better performance in the hub region; this was also related to the lower hub expansion ratio.

Due to the large number of geometric options in endwall profiling, even with regard to the profile features, it is difficult to make use of the above investigations to optimize the design of a contoured vane. Moreover, the results of different authors are not in a complete agreement and the loss reduction for a particular vane can not be predicted with reasonable accuracy. Therefore, according to Boletis, the only way to evaluate the potential benefits of a particular contouring is to support an analysis of the three-dimensional flow field, and to determine the actual losses by experimental testing.

Finally, in cooled gas turbines, a good knowledge of the 3-D flow field is an essential prerequisite for the design of an effective cooling system. The flow pattern close to the solid surfaces indeed determines the heat transfer coefficient distribution and, when film cooling is adopted, governs the interaction between the injected cooling air and the hot mainstream.

This paper presents the results of a detailed investigation of the flow field in contoured and planar cascades in linear configuration, by comparing the secondary flow development throughout the two cascades. The flow field inside the vane passages was analyzed by means of a 3-D Navier-Stokes code, while the flow evolution downstream of the trailing edge was surveyed by means of probe traversing.

The presented results aim to provide a contribution towards a better understanding of the complex 3-D flow configuration in contoured cascades, in order to give useful information to the designer of advanced gas turbines.

EXPERIMENTAL APPARATUS

Cascade Geometry

The investigation was carried out on two linear cascades formed with vanes scaled by the first stage of a large power gas turbine. One has a constant height with both flat endwalls, while the other presents a streamwise contraction of the span $h_2/h_2=0.70$, obtained by profiling the endwall at $z/h=1.0$. Both the cascades have the same pitch-chord ratio $s/c=0.812$ and the same outlet aspect ratio $h_2/c=0.751$. No restaggering of the vane was performed in the contoured cascade. A qualitative picture of the airfoil section and meridional flow path is presented in Fig. 1. In both cascades two airfoils were instrumented by means of pressure tappings at midspan, to get the airfoil pressure distribution.

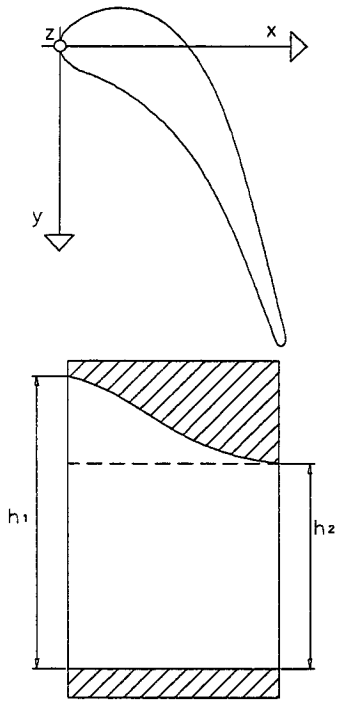

Fig.1 Blade and meridional profile

Wind Tunnel and Traversing System

Testing was performed in the high-speed wind tunnel for turbine cascades of the Politecnico di Milano; it is a blow-down type facility, equipped with large air storage, so that extensive 3-D flow surveys can be carried out. Downstream of the cascades, both composed of 7 vanes, there are two adjustable tailboards permitting a fine tuning of the side boundary in order to get acceptable flow periodicity conditions.

The measurements have been carried out by means of a miniaturized five-hole probe, characterized by a probe head diameter of 1.5 mm. Since the outlet flow is highly three-dimensional, the survey covered the whole flow field downstream of the trailing edge; the flow was traversed in five axial planes at $x/b= 1.10, 1.2, 1.35, 1.50$ and 1.65.

For this investigation a fully 3D traversing system was developed, allowing the probe automatic positioning in a defined three-dimensional grid of measuring points. By means of a four axis arrangement, based on stepping motors equipped with encoders, the probe can be displaced continuously not only along pitchwise and spanwise directions, but also in the axial direction. This is obtained by two eccentric rotations centered on parallel axis: the probe is mounted on a rotating probe-holder drum, and, at the same time, the probe can also be rotated around its stem. One of the advantages of this system is that the whole flow field can be investigated in a single run. The adopted measuring grid follows approximately the streamline pattern, in order to keep consistency between the results at different axial distances.

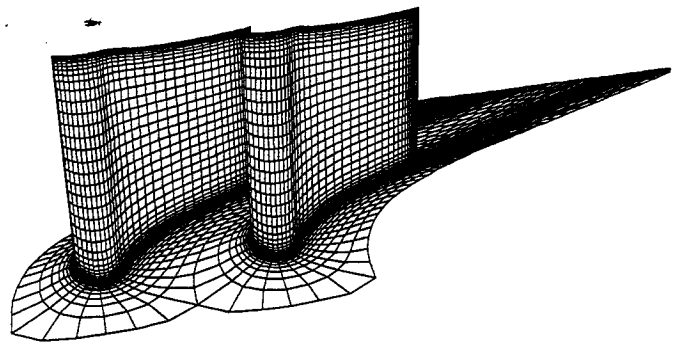

Figure 2 Contoured cascade: computational grid

In high gradient zones, typically in the wake near the trailing edge, significant errors in yaw angle and static pressure may arise, due to the finite distance between the probe holes, notwithstanding the small probe head dimension. To minimize this error, a post-processing procedure is utilized to determine the five pressure values in the same identical point; this is obtained by means of a bilinear interpolation of the probe pressure data over the measuring grid. Further details about the experimental apparatus and the data reduction may be found in Osnaghi and Perdichizzi (1990) and Dossena et al. (1996).

Test Program and Test conditions

The reference operating condition for this investigation corresponds to an outlet isentropic Mach number $M_{2is}=0.6$ and to an outlet isentropic Reynolds number, based on chord, $Re_{2is} = 1.08*10^6$; additional tests, not presented here, have been performed also at $M_{2is}=0.4$ and $M_{2is}=0.85$. The upstream flow was traversed by means of a flattened Pitot probe at $x/b=-0.8$. The inlet freestream turbulence intensity was 0.5% in both tests. Table 1 reports on the integral boundary layer parameters and inlet conditions, where boundary layer thickness is made non-dimensional with the channel half height. Note that, as expected, the integral value of the inlet loss is smaller for the contoured case; this is because the freestream velocity in the inlet duct is significantly lower, thus producing lower energy dissipation.

	z/h	δ^*	ϑ^*	H	Cpt_1/Cpt_d
CONT.	0-0.5	.0617	.0473	1.31	0.15
M_1=0.12	0.5-1	.0610	.0465	1.31	0.14
PLANAR	0-0.5	.076	.0532	1.44	0.27
M_1=0.16	0.5-1	.0775	.0542	1.43	0.27

Table 1. Upstream flow characteristics

NUMERICAL CODE

The code used in this work solves the full 3D Reynolds-averaged Navier-Stokes equations by means of a finite volume

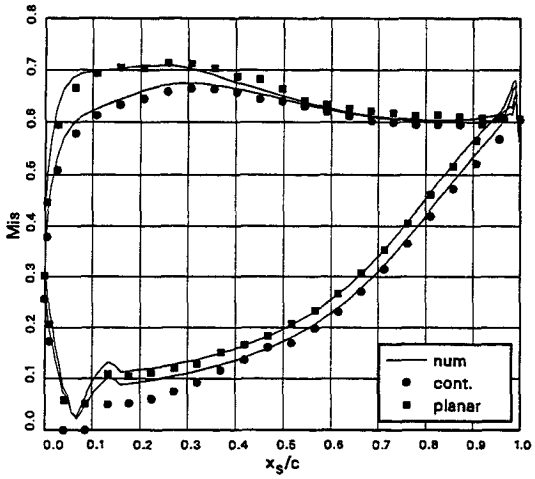

Fig. 3 Computed and experimental isentropic profile Mach number distribution at z/h = 0.50

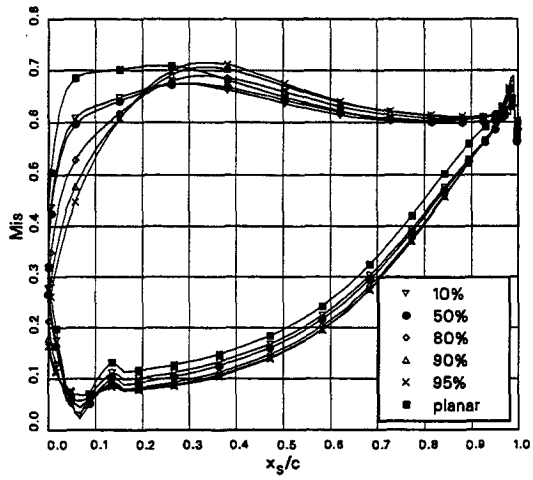

Fig. 4 Contoured cascade: computed isentropic profile Mach number distribution at different z/h.

explicit Runge-Kutta scheme. Acceleration to the steady state is enhanced by the use of local time stepping, implicit residual smoothing and V-cycle multigrid. The $\kappa-\omega$ turbulence model is used in its standard formulation (Wilcox, 1988). More details about the numerical discretization and the implementation of the turbulence model can be found in Bassi and Savini (1995). Using the low-Reynolds number version of the turbulence model (Wilcox, 1994), led in the contoured test case, due to the strong flow acceleration, to fully laminar boundary layers on the flat endwall and on the whole vane surface and to a fully laminar wake. It is quite difficult to presume that this latter result is correct, so the low-Reynolds formulation was discarded in favour of the standard one. As the inlet turbulence intensity in both cascades is rather low (around 0.5%), the imposed freestream value of ω in the computations was prescribed setting the ratio of turbulent to laminar viscosity equal to 0.01. This choice guaranteed from any unphysical change in the turbulent kinetic energy values near the inlet boundary. The measured spanwise total pressure profile was imposed at the inlet while spanwise uniform static pressure was fixed at the outlet of the computational domain, that extends more than one axial chord downstream of the trailing edge. The computational meshes consist of 220x32x72 hexahedral cells and are obtained by stacking the same C-type grid (220x32) with a fixed function of the non-dimensional height *z/h*. A plot of the grid used in the contoured case, showing half of the lines in each direction, can be seen in Fig. 2. Since the incoming boundary layer is not symmetric, the whole channel height was discretized in the flat cascade computation. The adopted clustering of mesh points near the solid walls, resulted in y^+ values lower than 6 in the blade-to-blade planes and lower than 12 at the endwalls. All computations were performed in single precision on a workstation HP735 and convergence was fixed when the root mean square of the time derivative of density was brought down to 10^{-4}.

RESULTS AND DISCUSSION

Airfoil Pressure Distribution

The key effect of endwall contouring is the modification of the pressure distribution with respect to the planar configuration. In fact a proper endwall design permits the reduction of the pitchwise pressure gradients in the first part of the flow channel, so to produce less intense secondary flow effects. The streamwise pressure distribution is also improved, leading to a lower inlet velocity and to a greater flow acceleration, so as to reduce vane and endwall boundary layers and the related losses.

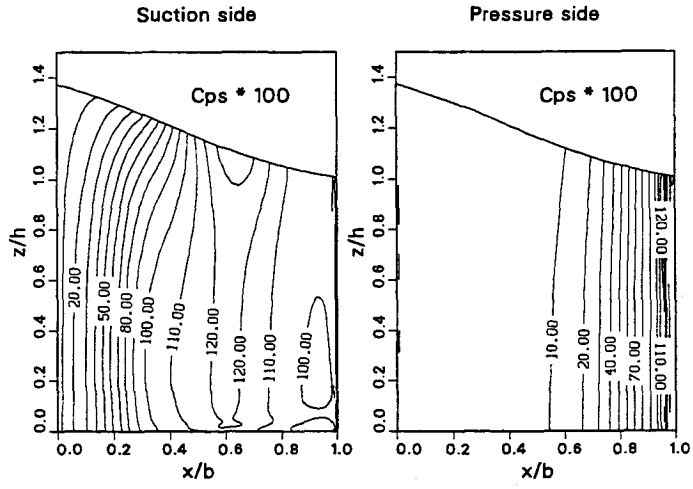

Fig. 5 Contoured cascade: computed pressure distribution on nozzle surfaces.

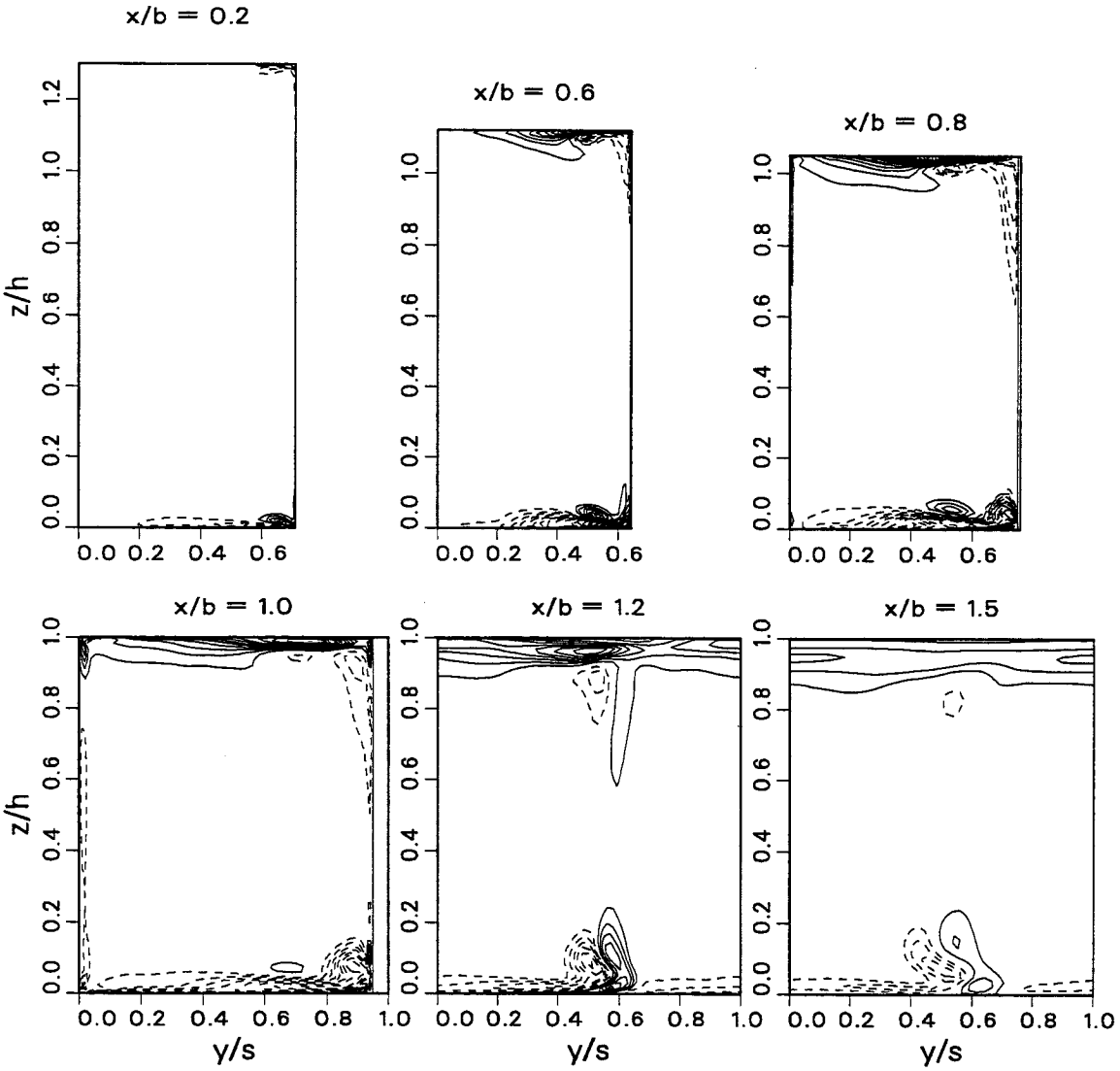

Fig. 6 Contoured cascade: computed streamwise vorticity contours (interval = 0.5; dashed = negative; channel pressure side = 0)

Fig. 3 presents the isentropic Mach number distributions measured and computed at midspan both for contoured and planar cascades. The major changes take place on the suction surface: lower velocities are found in the contoured case, being the major reduction in the front part of the profile; also the peak Mach number is reduced and its location is moved back, towards the trailing edge. As a result there is a lower diffusion rate over the whole rear suction surface, that is quite advantageous, relatively to the profile loss. As can be observed the computational results are in fairly good agreement with the experimental data. The computational code was used to determine the pressure field away from midspan, where pressure tappings were not available, and more generally to get the flow configuration inside the vane channel. Fig. 4 shows the computed profile Mach number distribution at different percentages of span. Approaching the contoured endwall the blade loading on the front part of the profile (up to 25% of the chord) is more and more decreased. This important unloading, occurring just where the flow undergoes the major turning, weakens the driving force responsible of the secondary flow development. Therefore much less intense secondary effects have to be expected on this side. On the flat side no appreciable variation with respect to midspan is observed.

The computed static pressure distributions on the nozzle surfaces, presented in Fig. 5 in terms of Cps, provide a comprehensive picture of the pressure field inside the channel. On the suction surface clearly appear the stagnation effect caused by the contouring, then the subsequent acceleration occurring at the change of the endwall curvature, and the final recompression approaching the trailing edge.

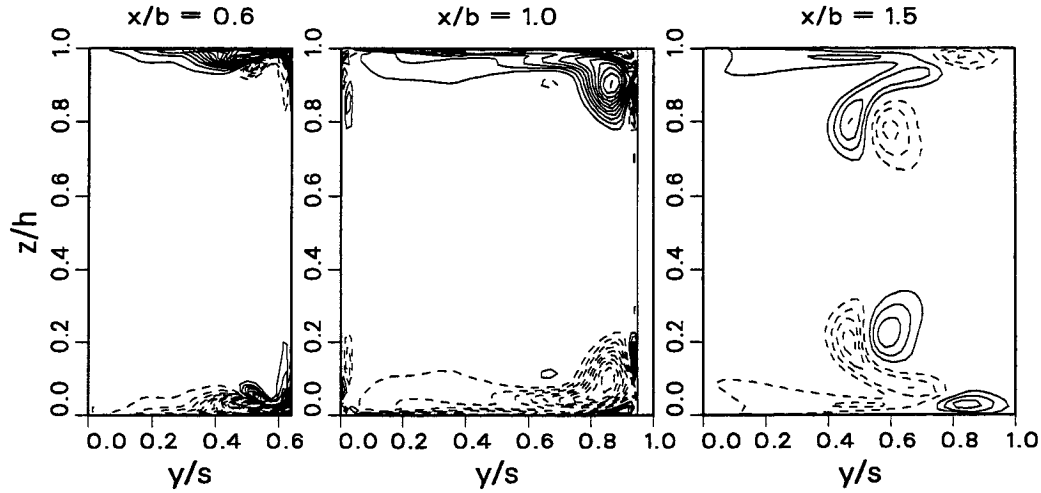

Fig. 7 Planar cascade: computed streamwise vorticity contours (interval = 0.5; dashed = negative; channel pressure side = 0)

Secondary Flow Analysis

The streamwise component of the vorticity vector ω_s, evaluated from the numerical results and made non-dimensional with respect to the chord and the outlet velocity, has been plotted for different axial planes. The plots for the contoured cascade presented in Fig. 6, allow one to follow the development of the secondary flows. In the first plane (*x/b=0.2*), at the hub there is a negative vorticity region across the passage, indicating the crossflow related to the formation of the passage vortex; a core with positive values, close to the suction surface, reveals the suction side leg of the horseshoe vortex.

At the tip only weak traces of negative vorticity are noticeable. Proceeding towards the trailing edge, at the hub one can observe the well-known secondary flow development, with the passage vortex core growing and moving towards the suction side. When the endwall crossflow impacts the suction surface there is a rapid enlargement of the negative vorticity region, that rises along the span. The positive core, on the opposite, weakens and it is moved away from the corner.

At the contoured endwall a similar behavior is observed up to *x/b=0.6*, but approaching the trailing edge a different configuration takes place. The vorticity core related to the passage vortex remains squeezed against the endwall, this being the combined effect of the spanwise pressure gradient and of the substantially higher acceleration which affects the endwall flow inside the channel. The stronger acceleration occurring at the contoured side actually produces a vortex stretching, so that at the trailing edge there is not a passage vortex as well defined as usual. Further reduction of the intensity of the passage vortex is caused by the lower blade loading occurring at the tip. However, the most interesting feature reported in Fig. 6 is that in the rear part of the suction surface a negative vorticity region is developing, so that in the exit plane an uncommon vortex configuration takes place with two main cores, both with negative vorticity, in the two halves of the span. The cause of this unusual vortex is the deflection which the vane suction side boundary layer undergoes, due to the endwall back curvature occurring from *x/b=0.6* and *x/b=1.0*. In fact, Fig. 5 shows that in this region acts a negative spanwise pressure gradient. Note also that here the flow is diffusing and the boundary layer is thickening. The net result is that there is a radial migration of low momentum fluid over the vane suction surface towards the tip. It is worth noticing that this is a non-viscous effect, just like the one producing the passage vortex. On the pressure surface this phenomenon is much less significant as the mainflow is accelerating up to the trailing edge and the boundary layer remains very thin.

In the planes downstream of the trailing edge, one can observe at the hub the presence of the trailing shed vortex and of the corner vortex, both with positive vorticity.

At the tip, the passage vortex remains confined close to the wall and it is swept away in tangential direction by the endwall crossflow. The negative vorticity core reduces rapidly and at *x/b=1.5* it has practically disappeared.

Fig. 7 shows the evolution of the streamwise vorticity distribution in the planar cascade. The patterns on both sides appear quite similar one to the other and resemble those taking place at the hub of the contoured cascade; however the vorticity levels are generally higher, indicating a larger intensity of the secondary vortices. Also the spanwise extent of the secondary effects is greater than in the contoured test case.

Downstream Flow

Figures 8 and 9 show the results of the area traversing in the measuring planes (located at *x/b=1.1, 1.2, 1.35 and 1.5*) in terms of total pressure loss, respectively for the planar and the profiled cascade. All loss coefficients are normalized with the profile loss of the contoured cascade, this being evaluated as

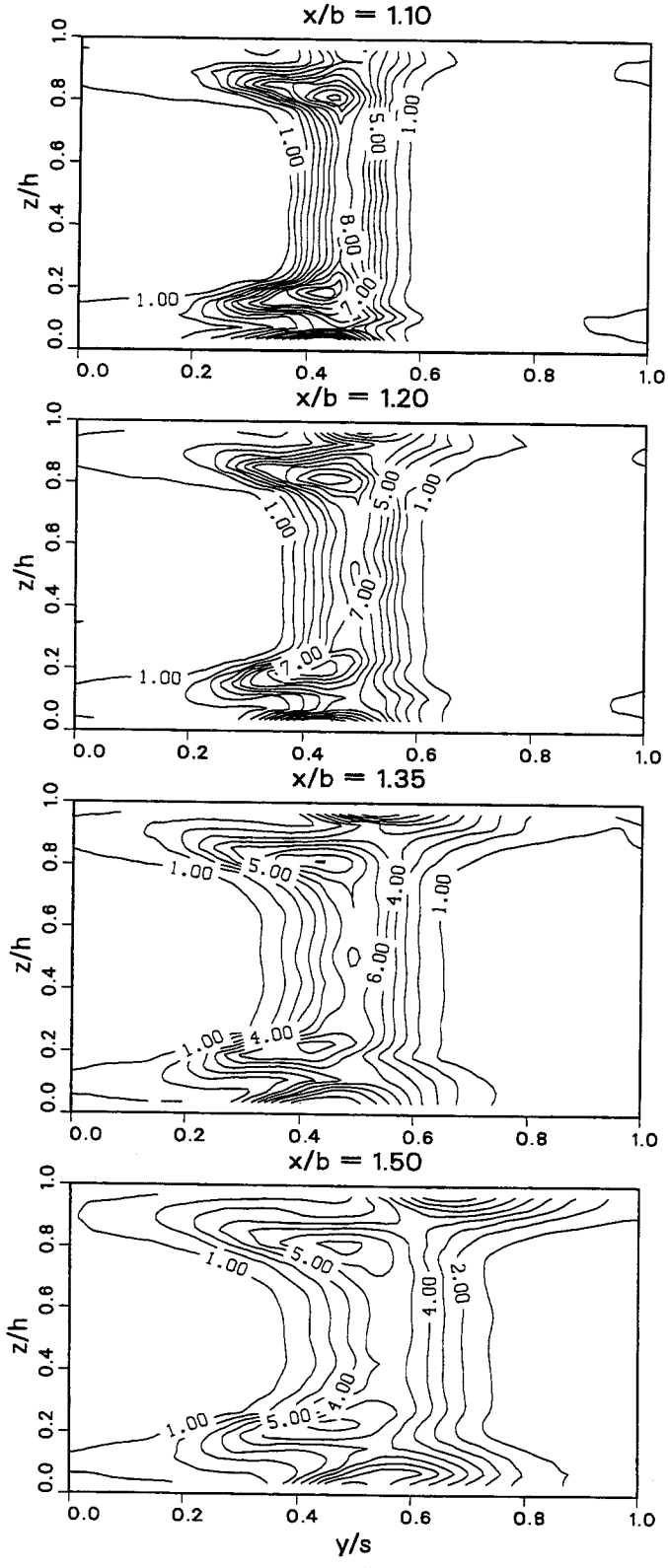

Fig. 8 Planar cascade: experimental total pressure loss contours on four downstream measuring planes

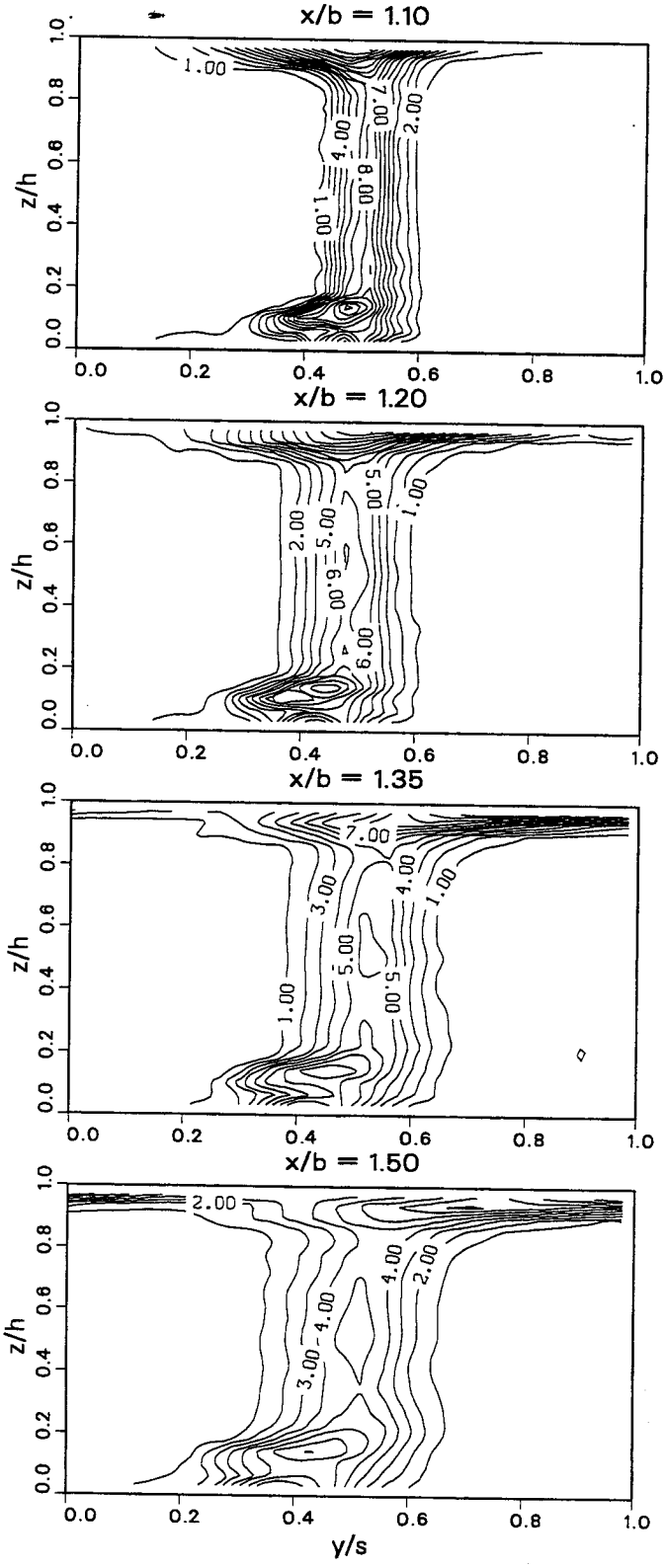

Fig. 9 Contoured cascade: experimental total pressure loss contours on four downstream measuring planes

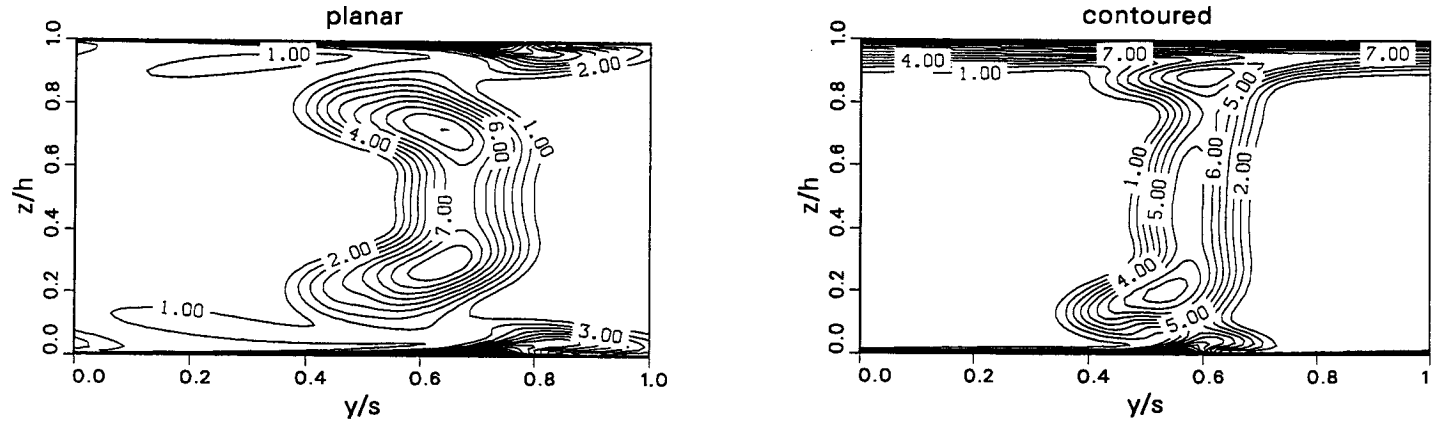

Fig. 10 Computed total pressure loss at x/b = 1.5

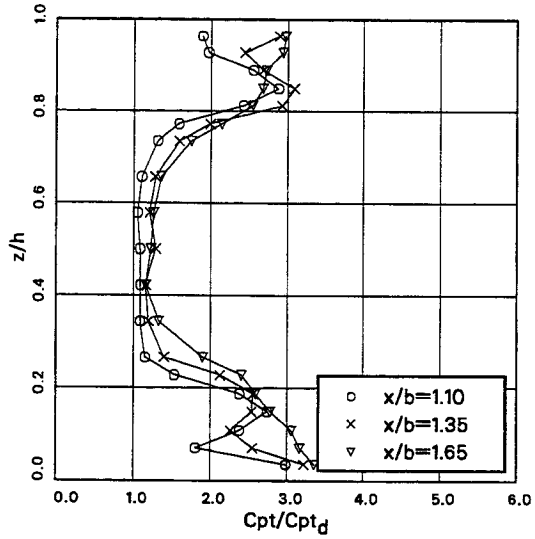

Fig. 11 Planar cascade: experimental pitchwise mass averaged total pressure loss.

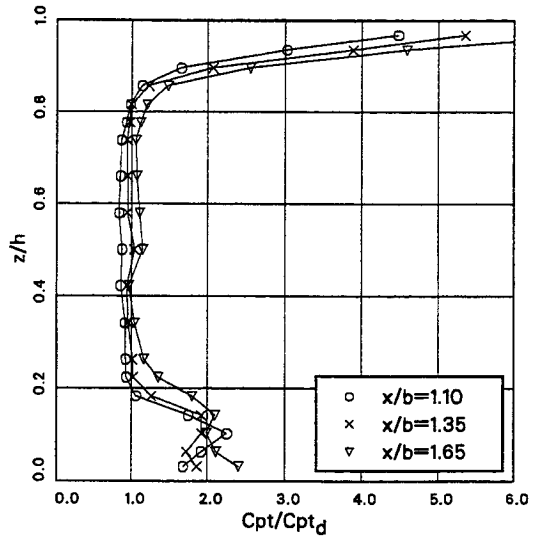

Fig. 12 Contoured cascade: experimental pitchwise mass averaged total pressure loss

the pitchwise mass averaged value over 30% of nozzle height about midspan. The contour plots of the planar case show a two-dimensional wake and almost symmetric patterns with respect to midspan; differences noticeable in the endwall regions can be addressed to some leakage due to imperfect sealing at the nozzle hub. One can observe the typical secondary flow configuration, with the low energy fluid region on the wake suction side and the loss core associated to the corner vortex close to the endwall. Moving downstream, the. flow undergoes an overall mixing process with a reduction ofhe loss peak values; the wake enlarges across the pitch and the secondary loss regions widen along the span

The results of the contoured cascade in the same planes evidence, as expected, a non-symmetric loss distribution. At the flat side (z/h=0), the loss contours resemble those of the planar case; the loss core related to the passage vortex is still present with roughly the same peak value, but its position is shifted towards the wall by approximately 10% of the span (e.g. z/h=*0.15* for x/b=*1.50*); the same happens to the loss core associated with the corner vortex, which turns out to be more confined in the endwall region. These effects are related to the stronger acceleration that the flow undergoes throughout the vane passage.

The loss distribution on the contoured side is significantly different: the loss contours are concentrated in the endwall region and only traces of a loss core squeezed against the wall are present. The comparison between flat and contoured case reveals that the transport of low energy fluid from the endwall boundary layer to the center of the channel is inhibited by the lower intensity of the secondary vortices. As a result, the total pressure loss distribution in the four planes resembles the one of a developing endwall boundary layer. This boundary layer

thickens considerably moving downstream under the influence of the recompression occurring at the tip.

Another important feature emerging by the comparison between Figures 8 and 9 is the reduction of the wake width: in the contoured case the tangential extension of the wake is smaller (in the last plane by about 10% of the pitch). This is a consequence of the reduction of the blade loading and of the smaller diffusion rate over the suction surface, which produce a more favourable boundary layer development, thus reducing the profile loss.

PLANAR ENDWALLS			
	z/h		
Cpt/Cpt_d	0 - 100 %	0 - 50%	50 - 100%
Overall	1.87	1.88	1.86
Profile	1.22	1.22	1.22
Net secondary	0.37	0.39	0.36

Table 2. Planar endwalls: mass averaged loss measurements at $x/b = 1.5$

CONTOURED ENDWALL			
	z/h		
Cpt/Cpt_d	0 - 100 %	0 - 50%	50 - 100%
Overall	1.38	1.33	1.45
Profile	1.00	1.00	1.00
Net secondary	0.24	0.18	0.30

Table 3. Contoured endwall: mass averaged loss measurements at $x/b = 1.5$

For the purpose of comparison, the computed loss contours for both cascades at $x/b = 1.5$ are shown in Fig. 10. As can be noted, the simulation catches all the relevant features discussed above. The main differences with the experiments concern the position of the vortex cores (shifted toward midspan in the numerical results) and the wake which appears to be thinner and with a greater energy deficit, as if it experienced a lower diffusion downstream of the trailing edge. This latter outcome is typical in the computation of turbine flows and is probably related to the inability of a steady-state computation to reproduce the enhancement in mixing caused by the actual unsteady vortex shedding. Anyway the simulations can be judged satisfactory and this confirms the usefulness of their use as a predictive tool for the field inside the vane passage.

Another consequence of the confinement of the secondary vortices induced by the contouring is the larger extension of the two-dimensional region in all the planes. This appears also from Figures 11 and 12, showing the spanwise distribution of the pitch averaged loss coefficient, respectively for the planar and the contoured case. The planar case reveals the typical secondary distribution of the mass averaged losses vs. span, characterized by a 2D region in the middle and by peaks near the endwalls. The contoured case shows a quite different loss distribution with a wider 2D region (60% of z/h, instead of 30%) and a lower level of the profile loss. Even on the flat side there is a lower loss level, meaning that the stronger acceleration of the flow through the cascade produces lower secondary losses. At the tip a very sharp increase of the loss

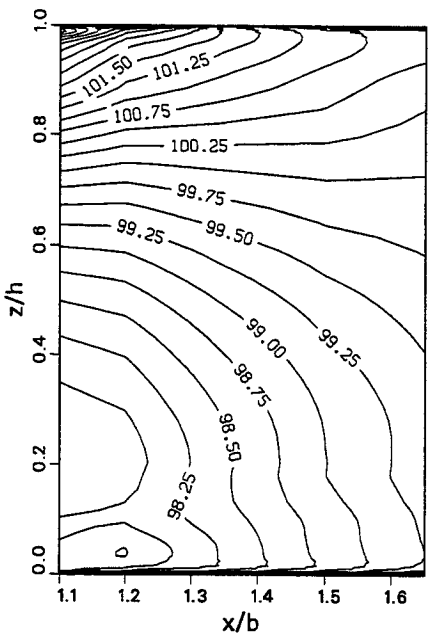

Fig 13 Contoured cascade: computed pitchwise mass averaged pressure contours (Cps*100)

coefficient takes place, so that the loss distribution looks like the one of an endwall boundary layer.

Tables 2 and 3 present the loss share for the two cascades, in the plane at $x/b=1.50$ for each half span. As already mentioned, the profile loss is defined as the (mass-averaged) loss over 30% of the nozzle height about midspan. The net secondary loss is obtained by subtracting the profile loss and the inlet loss (see Table 1) from the overall loss. The most relevant result shown in the tables is the significant reduction of the overall loss obtained for the contoured cascade. The overall loss reduction (-0.49) comes from the profile loss (-0.22), and in a minor part from to the inlet loss (-0.14) and from the net secondary loss (-0.13). The lower level of inlet and profile losses is clearly due to the lower velocity throughout the cascade and hence it can be considered a 2D effect. Moreover, the net secondary loss includes the endwall boundary layer dissipation. Therefore it can be concluded that the better cascade performance can not be related specifically only to a minor intensity or to a different structure of the secondary flows, but it is rather a global result connected to the

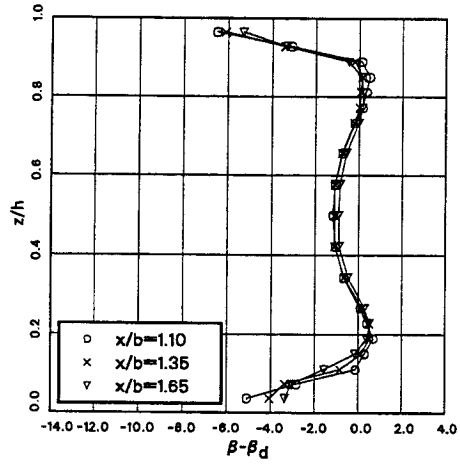

Fig. 14 Planar cascade: experimental pitchwise mass averaged outlet angle

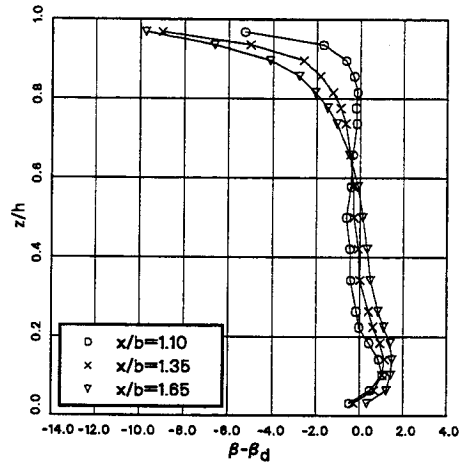

Fig. 15 Contoured cascade: experimental pitchwise mass averaged outlet angle

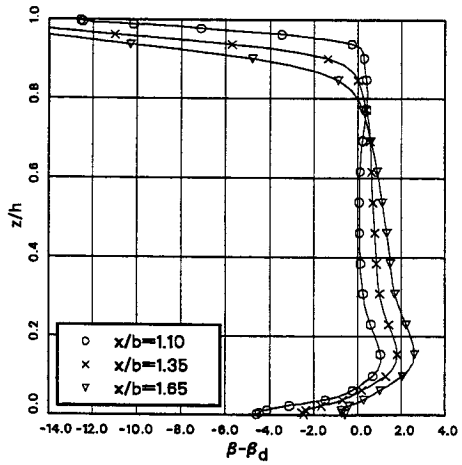

Fig. 16 Contoured cascade: computed pitchwise mass averaged outlet angle

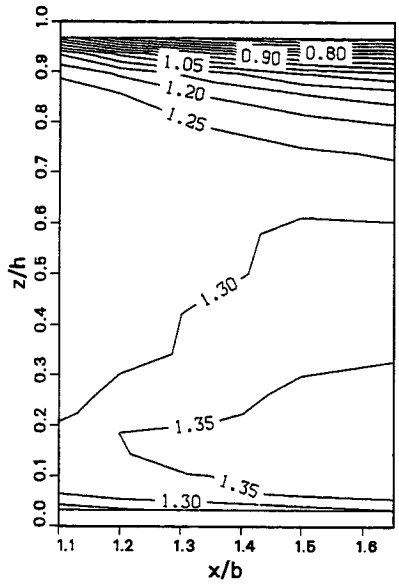

Fig. 17 Contoured cascade: experimental pitchwise mass averaged axial velocity density ratio contours.

substantial modification of the whole flow field.

In the planar cascade, the two halves of the span exhibit nearly the same amount of secondary losses, while, in the contoured cascade, the flat side performs considerably better, as also found by Kopper et al. (1981). This is mainly to be ascribed to two effects: one is the wider extension of the contoured wetted surface, the other is the adverse compression occurring at the tip downstream of the throat. Fig. 13, showing the computed isolines of pitchwise-averaged static pressure coefficient in the *x-z* plane, illustrates how, downstream of the trailing edge, the flow near the hub undergoes an acceleration and the flow near the tip a marked deceleration.

Spanwise Distribution of Averaged Flow Angle

The radial distribution in the measuring planes of the averaged outlet angle is presented for the two cascades in Figures. 14 and 15. The first feature emerging from the comparison between the two cascades is the increase of about one degree of the tangential flow angle at midspan for the contoured case.

The planar cascade exhibits the usual distribution connected to secondary flows with a substantial symmetry about midspan. In the first plane the maximum underturning angle is about 2 degrees while the overturning at the endwall is 4-5 degrees.

In the contoured cascade, only in the first plane there is a distribution resembling the one of the planar case with underturning and overturning regions. On the flat side there is a peak of underturning of about 2 degrees, but the 3D effects are confined close to the endwall, so that no overturning was found. On the opposite side the flow angle is practically

constant up to $z/h=0.85$ with only a slight underturning, but approaching the wall a significant overturning takes place. This is not a stable distribution, as in the following planes the outlet angle in the upper half channel reduces progressively causing a substantial overturning angle (up to 9 degrees). Finally, in the last plane there is a quasi-linear distribution over most of the span; this is confirmed also by the computational results presented in Fig.16. This kind of distribution is quite beneficial in the real engine; in fact, due to the increase of the peripheral velocity from hub to tip, it produces an improvement of the uniformity of the inlet flow angle to the following rotor.

The explanation for this uncommon decrease of the exit angle at the tip lies in the pressure field taking place downstream of the trailing edge (see Fig. 13). The pressure rise at the contoured endwall can in fact be obtained only at the expense of the axial velocity, being the tangential velocity fixed once outside of the vane, and therefore the flow angle decreases. Note that this is consistent with the axial velocity density ratio distribution, obtained by experimental data and shown in Fig. 17. As a result, there is an enlargement of the streamtubes located closer to the tip, which confirms the progressive reduction of the outlet angle.

CONCLUSIONS

The work presents the results of an experimental and numerical investigation carried out in order to clarify the effects of endwall contouring on the three-dimensional flow field in a gas turbine nozzle guide vane.

The comparison gives evidence that the streamwise contraction of the channel produces a substantially lower loss level, affecting secondary, profile and overall losses. The main cause of this reduction is the lower velocity inside the vane passage. In the contoured cascade, the flat side takes advantage of a stronger decrease of secondary losses, compared to the contoured side. This difference can be related to a poorer behavior of the endwall boundary layer, which on the contoured side undergoes a non negligible diffusion.

The secondary vortex structures are strongly affected by the endwall contouring: on the flat side the structure is similar to the typical configuration of straight cascades, but characterized by lower vortex intensity. On the profiled endwall, the contraction inhibits the formation of a proper passage vortex and its migration toward midspan; this is the result of an intense vortex stretching due to the local acceleration and of the deflection of the suction side boundary layer under the influence of the radial pressure gradient. It is felt that the endwall backward curvature near the trailing edge plays an important role in the vortex configuration and in the amount of tip overturning.

Another important consequence of the different flow field is the quasi-linear spanwise distribution of the outlet angle. This produces a more favourable inlet condition for the following rotor.

The resulting 3D-flow field, basically different from the one commonly found in planar cascade, is believed to have a strong impact on the design of an effective cooling system.

ACKNOWLEDGMENTS

The authors wish to thank ABB Power Generation Ltd for the permission to publish this paper.

References

Bassi, F., Savini, M., "Secondary Flows in a Turbine Cascade at Off-Design Conditions", AGARD CP-517, Loss Mechanism and Unsteady Flows in Turbomachinery, 1995.

Boletis, E., "Effects of tip Endwall Contouring on the Three-dimensional flow Field in an Annular Turbine Nozzle Guide Vane: Part 1-Experimantal investigation", *Journal of engineering for Gas Turbines and Power*, Vol. 107, pp. 983-990, 1985.

Dejc, E. et al., Atlas of Axial Turbine Blade Characteristic, Machinostroenie Publishing House, Moscow CEGB Inf. Services, C.E.Trans. 4563, 1965.

Dossena, V., Osnaghi, C., Perdichizzi, A., and Savini, M., "On Testing the Aerodynamics of Film Cooled Blades", Proceedings of the XIII Symposium on Measuring Techniques on Transonic and Supersonic Flows in Cascades and Turbomachines, Zurich, 1996.

Ewen, J. S., Huber, F. W., and Mitchell, J.P., "Investigation of the Aerodynamic performance of a small Axial Turbine", ASME Paper 73-GT-3, 1973.

Kopper, F. C., Milano, R., and Vanco, M., "Experimental Investigation of Endwall Profiling in a Turbine Blade Cascade, *AIAA Journal*, Vol.19. No.8,pp.1033-1040, 1981.

Morris, A. W., and Hoare, R. G., "Secondary Loss Measurements in a Cascade of Turbine Blades with Meridional Wall profiling", ASME Paper 75-WA/GT-13, 1975.

Moustapha, S.H., Williamson, R.G., "Effect of Two Endwall Contours on the Performance of an Annular Nozzle Cascade", *AIAA Journal*, Vol. 84, No. 9, 1986.

Osnaghi, C. and Perdichizzi, A., "Aerodynamic Measurements in Turbine Cascades at High Mach Number", Proceedings of the X Symposium on Measuring Techniques on Transonic and Supersonic Flows in Cascades and Turbomachines, Von Karman Institute Bruxelles, 1990.

Wilcox, D.C., "Reassessment of the Scale-Determining Equation for Advanced Turbulence Models", *AIAA Journal*, Vol.26, No.11, 1988.

Wilcox, D.C., "Simulation of Transition with a Two-Equation Turbulence Model", *AIAA Journal*, Vol.32, No.2, 1994.